Supporting information

Optimization of 5-hydroxymethylfurfural oxidation via photo-enzymatic cascade process

Marcelo A. do Nascimento,[a,b] Bernardo Haber, [a] Mauro R.B.P. Gomez, [a] Raquel A. C. Leão, [a] Mariusz Pietrowski, [c] Michał Zieliński, [c] Rodrigo O. M. A de Souza, [a] Robert Wojcieszak, [*b,d] and Ivaldo Itabaiana Jr [*b,e]

[a] BOSS Group - Biocatalysis and Organic Synthesis Group, Chemistry Institute, Federal University of Rio de Janeiro, Brazil;

[b] Univ. Lille, CNRS, Centrale Lille, Univ. Artois, UMR 8181 - UCCS - Unité de Catalyse et Chimie du Solide, Lille, France;

[c] Faculty of Chemistry, Adam Mickiewicz University, Poznań, Uniwersytetu Poznańskiego 8, 61-614 Poznań, Poland

[d] Université de Lorraine, CNRS, L2CM UMR 7053, F-54000 Nancy, France

[e] Department of Biochemical Engineering, School of Chemistry, Federal University of Rio de Janeiro, Brazil.

[*]Corresponding authors, *Robert.wojcieszak@cnrs.fr ivaldoufrj@gmail.com*

Summary

1. Synthesis of the g-C₃N₄

Graphitic carbon nitride was prepared by the pyrolysis of dicyandiamide (DCDA) (Sigma-Aldrich, Darmstadt, Germany, 99%) in a semi-closed system. In a 50-mL quartz crucible with a cover, 4 g of DCDA precursor was added and heated at 600 °C in a furnace for 4 h with a heating rate of 10 °C min^{-1} under ambient pressure in the air. After cooling to room temperature in the furnace, the obtained yellow material was ground into a fine powder in an agate mortar and labeled as gC_3N_4.

2. Synthesis of the 1%Pd/gC₃N₄

Metallic (Pd) photocatalysts were synthesized using the wet impregnation method. In 25 mL of water solutions of $PdCl_2$, 2 g of the graphitic carbon nitride powder (C_3N_4) was dispersed. The metal loading in the photocatalysts was 1.0 wt.%. The suspension was stirred for 2 h at room temperature and was subsequently evaporated. The samples were dried overnight at 80 °C and reduced at 300 °C for 4 h at a heating rate of 10 °C min^{-1} under ambient pressure in the presence of pure hydrogen.

3. Characterization

The photocatalysts were characterized by low-temperature N_2 adsorption, X-ray diffraction analysis (XRD), elemental analysis (EA), ultraviolet-visible diffuse reflectance spectroscopy (UV-Vis), and X-ray photoelectron spectroscopy (XPS).

The specific surface area (SSA) was determined by the Brunauer–Emmett–Teller (BET) method using a Micromeritics ASAP 2010 (Micromeritics, Norcross, GA, USA) surface area and porosity analyzer (surface areas were obtained from N_2-adsorption isotherms collected at 77 K). Cumulative pore volume and pore diameter were determined by Barrett–Joyner–Halenda (BJH) method from the desorption branch of isoterm.

The metal loading in the photocatalysts after reduction was determined using the inductively coupled plasma (ICP) method. An Agilent 720-ES ICP (Santa Clara, CA, USA) optical emission spectrometer combined with a Vulcan 42S robot was used to determine the Pd loading. The measured metal contents were close to those assumed and amounted to 0.82 wt.%.

The XRD analysis was performed in the 2θ range between 6° and 40° on a Bruker D8 Advance diffractometer (Billerica, MA, USA) using CuKα radiation. Bragg's law $n\lambda = 2d\sin\theta$ (where n is an integer, λ is the radiation wavelength (λ = 1.5418 Å), and θ is the reflection angle for the reflex hkl) was used to calculate the distance d_{hkl} for the sample. The crystallite size of g-C₃N₄ was calculated using the Scherrer formula $D = K\lambda/\beta\cos\theta$, where D is the crystallite size in nm, K is the Scherrer constant (0.94), λ is the radiation wavelength (λ = 1.5418 Å), and β is the full width of the (002) crystallite peak at half maximum.

The UV-Vis diffuse reflectance spectra were recorded on a Jasco (Tokyo, Japan) model V-670 spectrophotometer.

The XPS analysis of the catalysts was performed using a Kratos Axis Ultra spectrometer (Kratos Analytical, Manchester, UK). The excitation source was a monochromatized aluminum X-ray source (Al Kα (1486.6 eV) operated at 10 mA and 15 kV. The charge referencing method used was the C (C, H) component of the C 1s peak of adventitious carbon fixed at 284.5 eV. Spectroscopic data were processed by CasaXPS ver. 2.3.17PR1.1 software (Casa Software Ltd., Teignmouth, UK) using a peak-fitting routine with Shirley background and asymmetrical Voigt functions.
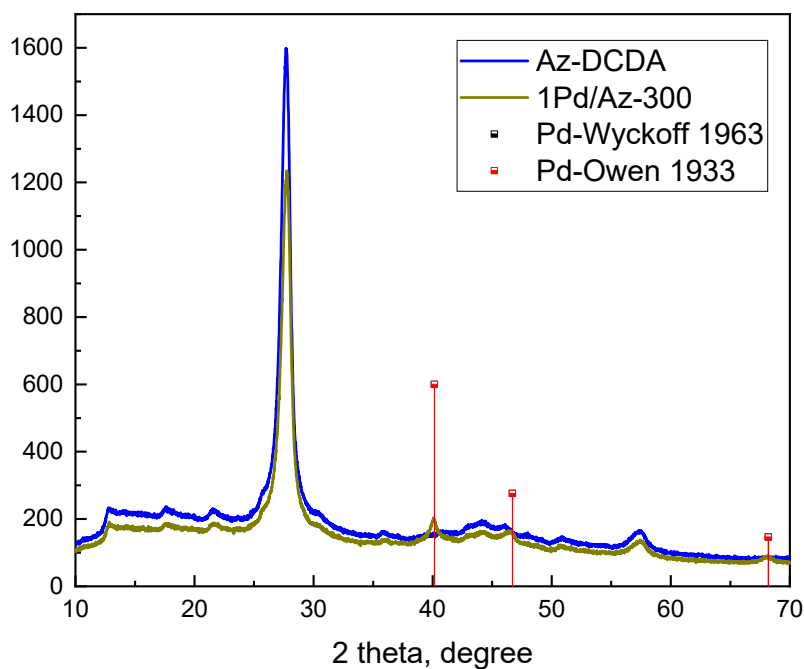
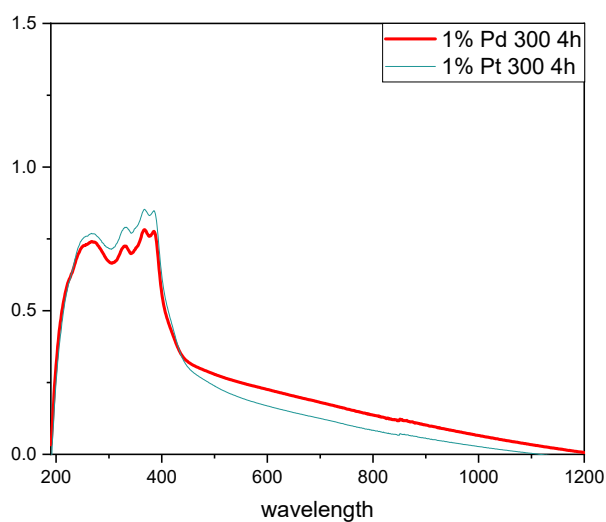Figure S.1: XRD patterns of the catalysts.

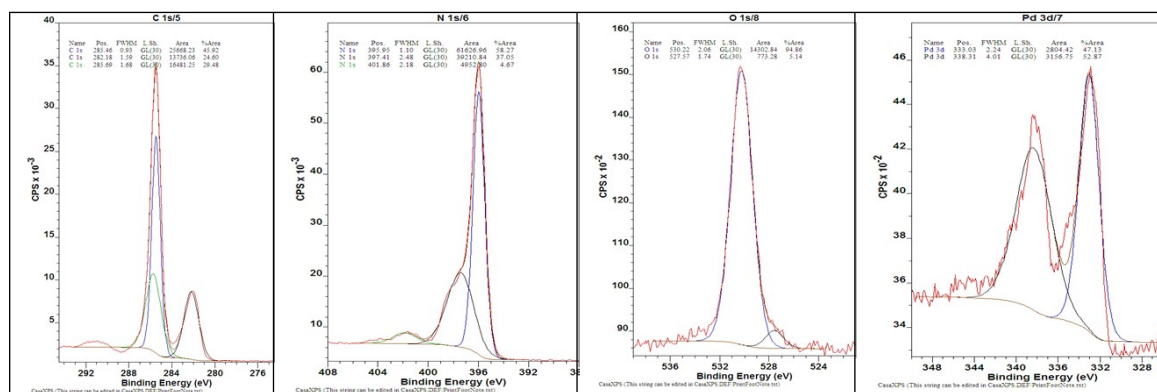Figure S.2: Uv-Vis spectra of the catalysts reduced at 300 and 400°C.

Figure S.3: XPS spectra of the C1s, N1s, O 1s and Pd 3d regions.

Using the impregnation method, the active phase envelops the support surface. Consequently, it is anticipated that the surface area will decrease after metal deposition compared to the pure support. This decline is attributed to the potential blockage or filling of pores in the support by the active phase. However, upon depositing Pt-group metals, an unexpected increase in the surface area of the photocatalyst was observed. The specific surface area of the 1%Pd/gC3N4 catalyst after H2 reduction was 53.7 m^2/g which was much higher than the surface of the pristine gC3N4 (28,5 m^2/g).

The observed increase in surface area cannot be solely attributed to the presence of the metal phase in the catalytic system. It must be linked to structural alterations in the support. One plausible explanation involves changes in the support structure during the photocatalyst's reduction at 300 °C for 4 h in a hydrogen flow. In this process, the graphitic carbon nitride (organic polymer) is exposed to atomic hydrogen, an aggressive reducing agent generated on the metal surface during reduction. Platinum-group metals, known for their high activity in hydrogenolysis and hydrogenation reactions, can induce hydrogenolysis and hydrogenation of the C−N bonds in the vicinity of metal particles, leading to partial etching of g-C3N4. Consequently, this process generates new pores and structural defects, resulting in an increase in specific surface area (SSA). The porosity and SSA results clearly indicate that g-C3N4 undergoes structural changes during the photocatalytic reduction process, leading to an increase in SSA.

Diffractogram shown on Figure S1 exhibits two distinctive reflections of carbon nitride. The first reflection (2θ = 27.7°) corresponds to the (002) crystallographic plane, signifying the interlayer stacking of aromatic rings. The second reflection (2θ = 12.8°) corresponds to the (210) plane and is associated with the in-plane structural packing motif of tri-s-triazine units in melon (separation between parallel melon chains). The intensity of the reflection at ~27.7° (002) in the diffractograms of

the photocatalysts is marginally lower than that of the support, and simultaneously, its full width at half maximum (FWHM) increases. Using the Scherrer formula, the size of the g-C3N4 crystallites was estimated from the FWHM. For the metallic photocatalysts, the size of the g-C3N4 crystallites was slightly smaller than that of the CN (or CNr) support. The number of layers constituting the carbon nitride crystallite was calculated by dividing the size of g-C3N4 crystallites by the interplanar distance d. The number of layers was approximately 30 for CNr and around 29 for the Pd modified photocatalysts (rounded up to unity). This indicates a minor disruption in the large-scale structure of carbon nitride.

The UV-Vis spectra of the photocatalysts (Figure S2) reveal a distinctive band in the 190–450 nm range, corresponding to the aromatic structures in g-C3N4. All UV-Vis spectra exhibit two characteristic peaks: the first around ~250 nm, attributed to the $\pi \rightarrow \pi*$ transitions in aromatic rings, and the second around ~380 nm, associated with electron transitions from the nonbonding orbitals of nitrogen atoms to the antibonding aromatic orbitals. An augmentation in absorption in the visible range beyond 600 nm, known as the Urbach tails, was observed for all photocatalysts. In comparison to C3N4, metallic Pd photocatalysts display a visibly broader and stronger absorption tail extending to 1000 nm, attributed to the defect-related states within the band gap. The heightened light absorption may lead to an increased number of electron–hole pairs under visible light, enhancing the effective absorption of radiation by the photocatalysts and consequently elevating their activity.

X-ray photoelectron spectroscopy (XPS, Figure S3) proves to be a highly valuable technique for the advanced characterization of g-C3N4 materials. Typically, the N 1s spectrum reveals four signals attributed to pyridinic nitrogen in the heptazine ring (398.6 eV; labeled Py), primary amine -NH2 (399.3 eV; labeled NH2), secondary amine -NH- (400.3 eV; labeled NH), and quaternary nitrogen arising from the N-(C)3 component (401.4 eV; labeled Q). In the case of the Pd photocatalysts, an increase in the amount of −NH2 nitrogen was noted. It confirms that Pd predominantly catalyzes the hydrogenolysis of the aromatic N−C=N bond.
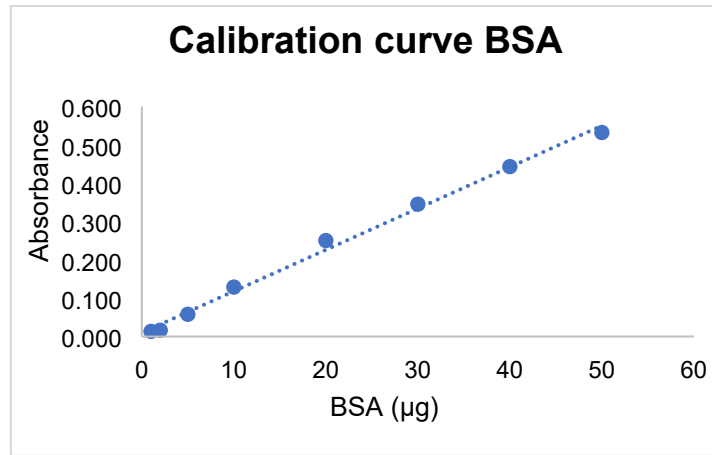
4. Calibration curve BSA

Figure S.4: Calibration curve obtained for different concentrations of bovine serum albumin (BSA) using the Bradford method.

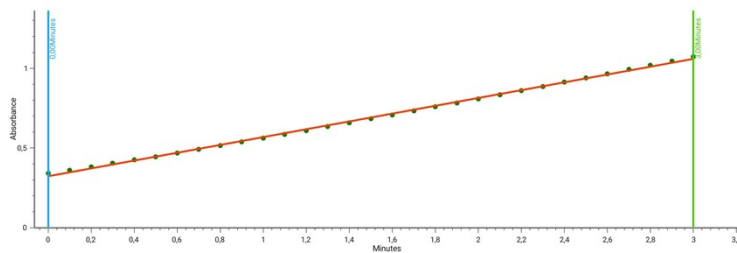## 5. Kinetic test for laccase activity through ABTS oxidation

Figure S.5: Kinetic analysis in GENESYS™ 150 UV-Vis spectrophotometers after 3 minutes of ABTS oxidation in orbital shaker at 30°C and 400 rpm by free laccase without stop reaction.
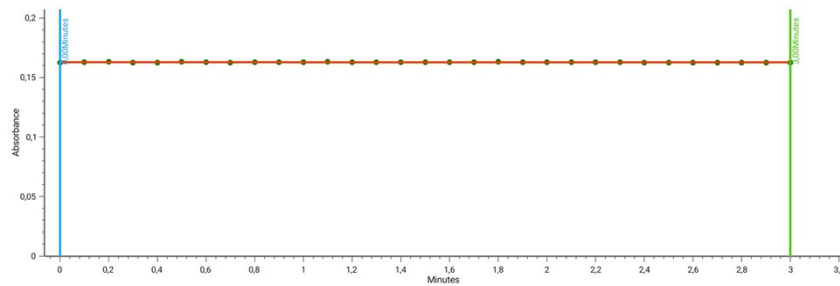

Figure S.6: Kinetic analysis in GENESYS™ 150 UV-Vis spectrophotometers after 3 minutes of ABTS oxidation in orbital shaker at 30°C and 400 rpm by free laccase with stop reaction.

6. Quantification of HMF, DFF, FFCA, HMFCA and FDCA by HPLC
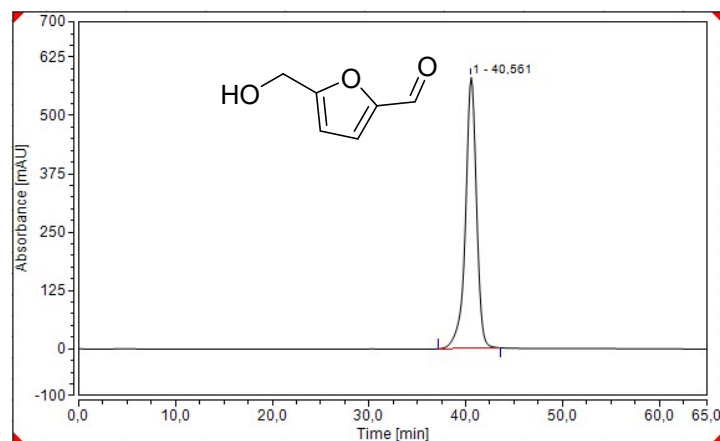
Figure S.7: Chromatograms with the HMF standard.
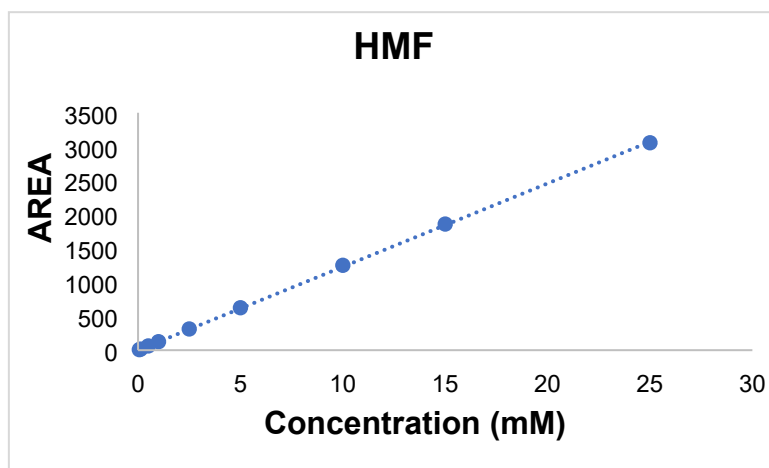
Figure S.8: Calibration curve obtained for different concentrations of HMF using commercial standard.
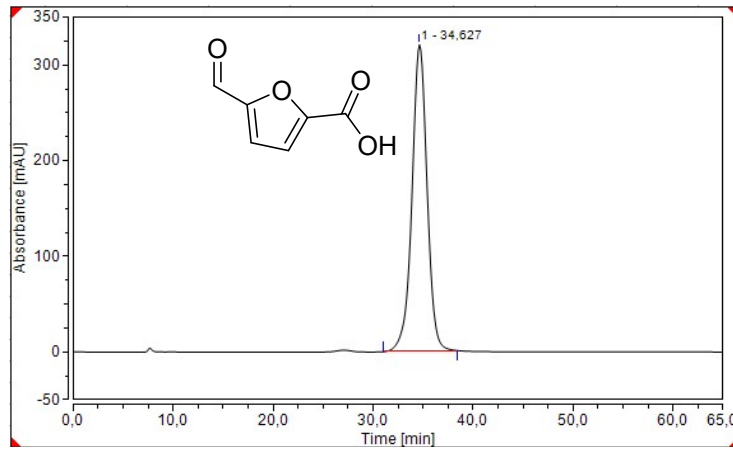
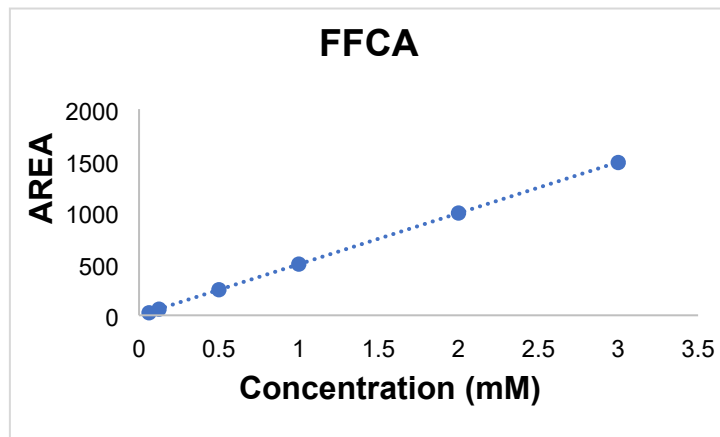Figure S.9: Chromatograms with the FFCA standard.

Figure S.10: Calibration curve obtained for different concentrations of FFCA using commercial standard.
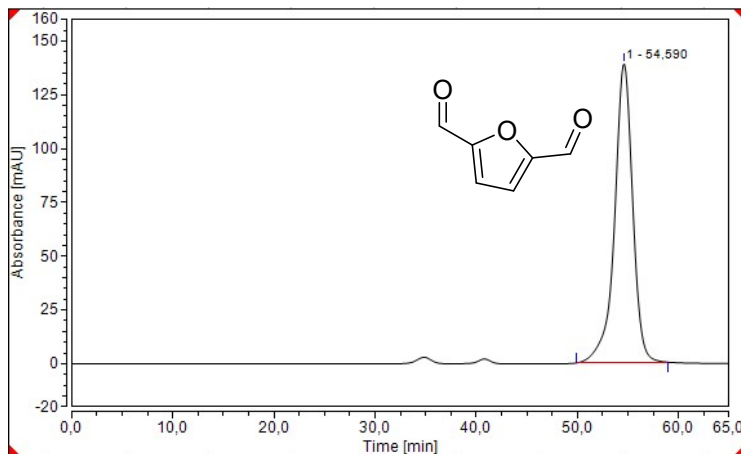

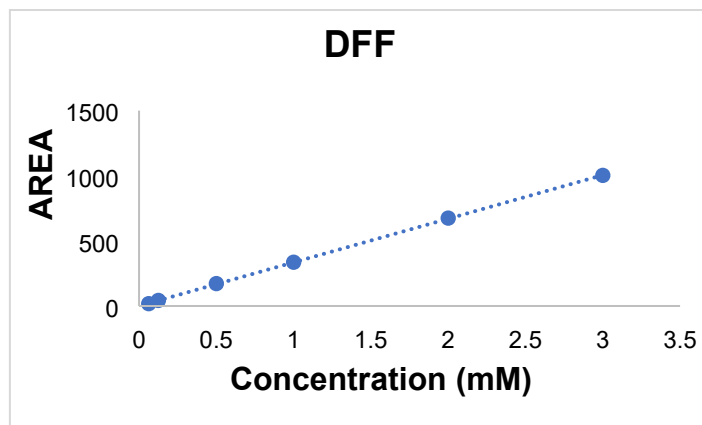Figure S.11: Chromatograms with the DFF standard.

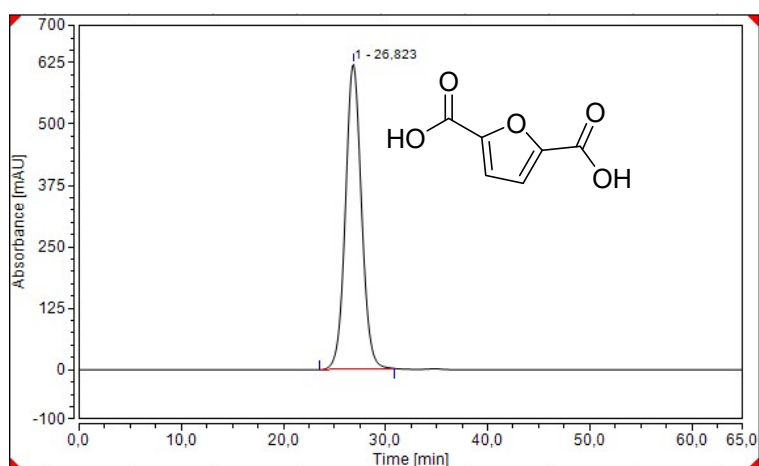Figure S.12: Calibration curve obtained for different concentrations of DFF using commercial standard.

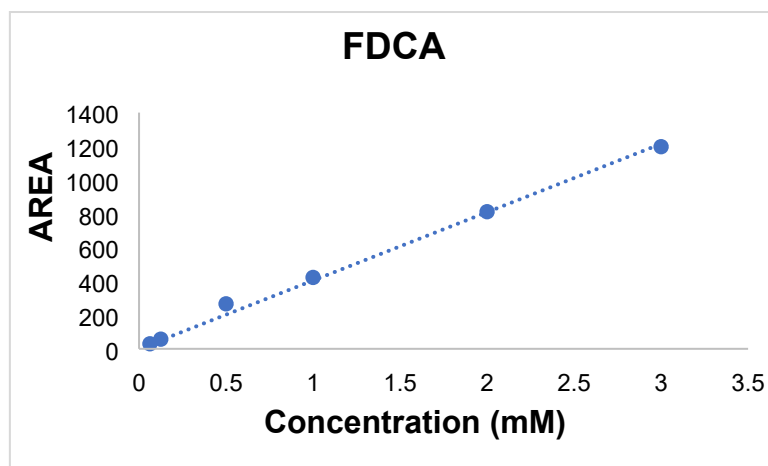Figure S.13: Chromatograms with the FDCA standard.

Figure S.14: Calibration curve obtained for different concentrations of FDCA using commercial standard.
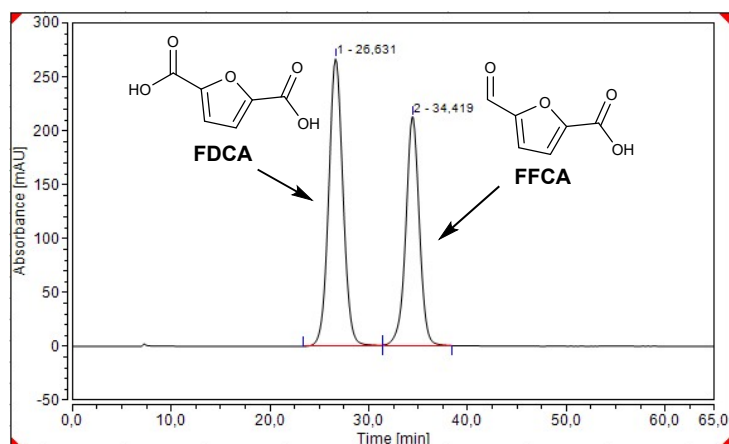
Figure S.15: Representative chromatogram of the batch reaction with Lac*TV*.

Table S.1: Results of HMF oxidation reaction using *Unit 1* (Configuration A).

Entry	Catalyst	HMF (mM)	Conversion (%)	Selectivity (%)				
				DFF	HMFCA	FFCA	FDCA	BY-PRODUCTS
1	gC₃N₄	25	18	**83**	2	9	0	6
2		75	13	**77**	6	8	0	9
3	gC₃N₄/Pd1%	25	26	**72**	3	**19**	0	6
4		75	13	**67**	**11**	9	0	**13**

Condition: Initial HMF concentration (25mM or 75 mM); TEMPO (0.3 equivalent); Citrate buffer pH 6.0 (75mM); Blue light (460 nm); 500 rpm; reaction time (2h); and Catalyst (10 mg) and Room temperature.

7. Determination of productivity

In batch

$$Productivity\ (P): \frac{V * C_r * f_r * \left(\dfrac{PM_{PROD}}{PM_{REAG}}\right) * conv * sel}{100 * m_A * T} \qquad \text{(Equation 1)}$$

In flow

$$Productivity\ (P):\ \frac{F * C_r * f_r * \left(\dfrac{PM_{PROD}}{PM_{REAG}}\right) * conv * sel}{100 * m_A}$$

(Equation 2)

Where, **V** is the reaction volume (mL), **F** is the flow rate (mL.min^{-1}), **T** is the reaction time, Cr is the concentration (mg.mL^{-1}), fr is the purity HMF (%), P_{MPROD} and P_{MREAG} are molecular weight of product and reagent (g.mol^{-1}), respectively, $conv$ is the conversion (%), **sel** is the selectivity for products (%), m_A is the mass of biocatalyst.